DEVELOPMENT OF A SYSTEM FOR AERODYNAMIC FAST-RESPONSE PROBE MEASUREMENTS

C. Gossweiler; H. Humm; P. Kupferschmied

ETH; Swiss Federal Institute of Technology Institute of Energy Technology
Turbomachinery Laboratory, Prof. Dr. G. Gyarmathy
Zürich, Switzerland

ABSTRACT

This paper describes the development of a fast-response probe measurement system. Small pressure probes have been equipped with up to 4 miniature pressure sensors. The high frequency response of such sensors allied to minimized cavities between the flow and the sensing diaphragm enables the probe system to take measurements up to 40 kHz bandwith (typical blade passing frequency: 2-10 kHz).

First results of investigations on the aerodynamics of high frequency response measurement probes are presented including experiments in a water towing channel with unsteady flows around different probe geometries. The packaging of the sensor chip into the probe, the properties of the sensors and the measurement errors are examined. Probe calibration methods and aerodynamic evaluation procedures are discussed, followed by a presentation of the data acquisition system and of the data evaluation software. Measurements in a radial compressor test rig and in a fully devoloped pipe flow are shown as applications.

1 INTRODUCTION

Many authors have shown that a better insight into the flow conditions of thermal turbomachines (e.g. jet engines) is a key to improve both performance and safety. The knowledge of the unsteady flow-patterns through the rotating components permits to (in)validate numerical flow computational codes, to make more accurate predictions and enhancements of new designs and to reduce undesired effects like stall, surge or blade flutter.

The development of aerodynamic fast response probes first became possible twenty years ago with the availability of miniature silicon pressure sensors. Because of the relatively large sensor sizes in the first multihole probe applications the sensors were located in the probe shaft (MATSUNAGA et al.1978). With the increased miniaturization of the sensors the trend was to place them as close as possible to the measuring point and thus enhance the bandwidth of the measurement (KERREBROCK et al. 1980, HENEKA 1983, SHREEVE-NEUHOFF 1984, EPSTEIN 1985).

One of the main advantages of fast response aerodynamic probes compared with hot wires is their high robustness and insusceptibility to dirt-contamination. In contrast to the highly sophisticated nonintrusive laser techniques (LDA/L2F) fast response probes are easier to use for measurements in turbomachines and provide a higher signal-to-noise ratio. An additional feature of this technique is the ability to determine not only the unsteady flow vector but also the time dependent static and total pressure of the flow.

Although the problem has been identified earlier by several authors to the present little attention has been paid to the dynamic aerodynamic flow characteristics around probes in fluctuating flow fields. An investigation concerning the dynamic calibration of aerodynamic probes is described in section 2 of this paper.

One of the major objectives of this work is to minimize the size of intruded probes. This will lead to enhanced spatial and time resolution of the measurement with reduced dynamic aerodynamic errors and flow disturbances. Section 3 describes the construction required and shows that with an optimal packaging technique the errors of the pressure measurement can be reduced.

After the calibration of the sensors the probes can be aerodynamically calibrated in a wind tunnel. Adequate model equations have to be chosen to fit the aerodynamic properties of the probe in the interesting angular range with high accuracy. Either an iterative or direct data evaluation can be used. With the latter method the computational time is reduced but the angular range restricted.

Measuring equipment and data evaluation are described in section 5. Two examples of applying the measurement-system for flows in a radial compressor and turbulent pipe-flow are presented in section 6.

2 AERODYNAMIC CONSIDERATIONS FOR FAST-RESPONSE PROBE-DESIGN

In order to optimize the design for fast-response probes the fundamental *static and dynamic* properties of bluff bodies (prismatic probes) have been aerodynamically studied.

2.1 Static Calibration of Aerodynamic Probes

From a series of cylindrical probes (fig. 2-1) calibration data were recorded in a closed-walled wind tunnel (0.3<Ma<1.2). The evaluation of the data was performed with emphasis on:

- *Calibration range* which must be greater than the maximum incidence angle encountered during measurements in turbomachines. Increasing the apex angle of wedge probes leads to extended calibration ranges. A dramatic increase is obtained by placing the sensing hole to the rear (l/L=0.25) of the probe or by shaping the probe round-nosed (fig. 2-2).

• *High Sensitivity* improves the angular resolution of the measurement. It was found that a probe with a nose radius of 20% of its total length (nr. 4, fig. 2-2, part C) exceeds the sensivity of all other configurations tested.
• *Mach number dependence* on static pressure coefficient and sensitivity (fig. 2-3). The true static pressure can be measured by using circular cylinders (nr. 7, fig. 2-3 for 0<Ma<0.5) or wedge-type probes with either very small total apex angles or sensors located to the rear of the probe's body (nr. 2, fig. 2-3). For various applications yaw meters indicating the true static pressure of the free stream are desirable, although for our applications (see chapter 4) where probes are thoroughly calibrated a clear relation of the static pressure coefficient K_s(Ma, yaw- and pitch-angle) can be determined. Another indication of influence of Mach number on probe calibration can be seen from figure 2-3 showing the change of sensitivity dcp/dα versus Mach number. Ideally a probe should show a constant value over the whole Mach number range.

The geometric parameters varied were a) total apex angle of probe from 45 to 90° (probe nr. 1, 5 & 6); b) locations of sensing hole (probe nr. 1 & 2); c) nose radius of probe in % of total length from 0 to 20% (probe nr. 1, 3 & 4) and d) circular cylinder (probe nr. 7).

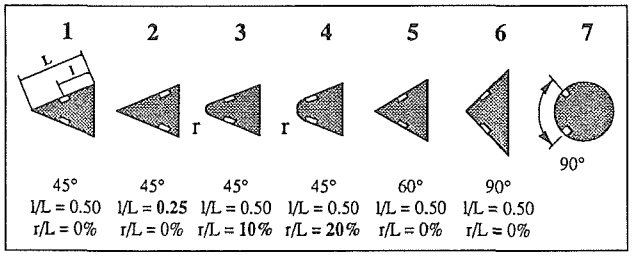

Figure 2-1 *Probes tested in air flow from 0.2<Ma<1.2*

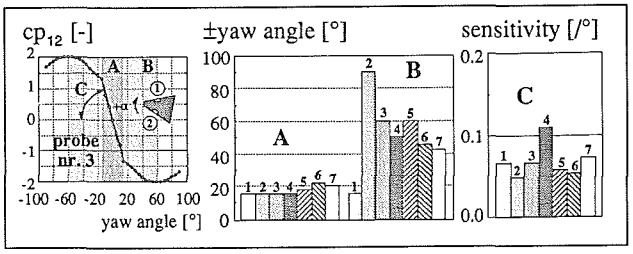

Figure 2-2 *Calibration range for the probes tested (A: quasi-linear; B: unambiguous and C: sensitivity) for a free stream Mach number of Ma = 0.5*

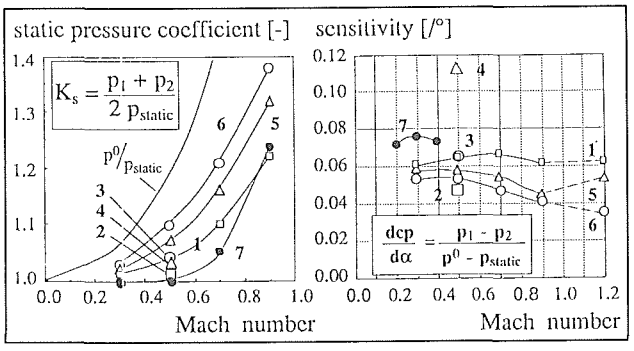

Figure 2-3 *Static pressure coefficient and sensitivity dcp/dα versus Mach number*

2.2 Dynamic Calibration of Aerodynamic Probes

By intruding aerodynamic probes for measurements into turbomachines these devices face highly turbulent flows with fluctuations in magnitude and direction. In such cases with application of static calibration data large *dynamic errors* occur which considerably aggravate the quality of the flow measurement. The total dynamic error is a sum of errors due to interactions between shed vortices and flow on the probe's surface, fluctuations of the flow-vector's magnitude and directional oscillations.

• *Vortex Interaction Errors*

Shed vortices from bodies immersed into a uniform flow generate pressure fluctuations on the surface. Such fluctuations can be mistakingly interpreted as oscillations of the incidence-angle. For bodies with a fixed separation point (e.g. wedge-type probes) these interaction-effects are lower.

• *Fluctuations of Magnitude of Flow Vector*

KOVASZNAY et al. 1981 reported that the pressure distribution around spheres (radius a) in flows fluctuating in magnitude are proportional to a term containing the squared velocity u^2 and a second with the acceleration du/dt:

$$p = \overline{p_{static}} + A\frac{\rho}{2}u^2 + B\,\rho\,a\frac{du}{dt}$$

If the *forces* on bodies are considered, the constant B is called "added-mass-coefficient". KOVASZNAY et al. found that B = 0 at parts of the surface where for nonfluctuating flows the true static pressure of the free stream is registered. Ideally the sensing holes should be placed in these areas to minimize dynamic errors due to added-mass effects.

• *Directional Fluctuations of Flow Vector*

Dynamic flows comprise a number of phenomena like a) conceptual differences between static and dynamic boundary-layer behaviour and separation; b) unsteady stall phenomena; c) rotational added-mass effects; d) coupling between shed vortices from the probes and the cyclic flow field on the probe body.

a) Dynamic Boundary Layers: Several authors (e.g. SEARS/TELIONIS) found that in dynamic flows the classical Prandtl's law for boundary layer separation loses its validity. Whilst for static flow conditions the boundary-layer will separate when the wall shear-stress becomes zero, thin layers of reversed flows may exist in dynamic flows without disturbing the "outer flow". Analysis by McCROSKEY 1975 revealed that during the loop of oscillation of a body the unsteady response of the boundary-layer will alternately lead or lag the "quasi-static" case. Generally a delay of flow-separation can be observed in unsteady flows (TELIONIS, SARPKAYA, NASH-SCRUGGS).

b) Unsteady Stall: According to CARR/McALLISTER-McCROSKEY the phenomenon of dynamic stall for NACA 0012-profiles occurs due to a separated vortex propagating rearwards from the leading edge resulting in transient pressure distributions along the surface of the profile promted by the bursting of a laminar separation bubble (BEDDOES). Classical dynamic stall effects occur only in cases where the static stall angle is exceeded.

c) Added Mass Effects: Forces acting on the probe due to rotational displacement of fluid analoguos to translatory oscillations. The effect is high for small-angle wedge probes but zero for circular cylinders.

d) Coupling of Shed Vortices occurs in cases where the frequency of the flow fluctuation is close to the natural shedding frequency of the vortices. In this case ("lock-on") the dynamic conditions differ from others below or above the critical case.

2.2.1 Experiment

The experiments described herein are confined to rotational oscillations of flows around probes; experiments on translatory fluctuations are in progress.
The aims of the tests performed at our laboratory are to experimentally determine the quantitative dynamic calibration data of different probe geometries by varying the frequency and amplitude of the oscillating free stream at levels typical of turbomachines.

2.2.2 Experimental Setup

The probe sizes used for fast response measurement in turbomachines are usually of the order of 1< d< 6 mm depending on the number of sensing holes. With the ground harmonic frequency of the flow fluctuations being identical to the blade-passing frequency f in the kHz-domain, velocities u ranging from 100 to 300 m/s, the characteristic nondimensional parameter k (reduced frequency) can be determined:

$$k = \frac{f \cdot d}{u} \approx 0.05 - 0.5$$

To avoid having to create well known oscillatory flows in the kHz-domain the experiments were performed in a water-towing-channel. Using probes of about 30 mm width (velocities 1<u<5 m/s, frequencies 1<f<10 Hz) the dynamic similarity (reduced frequency, Reynolds number) was satisfied.

By instantaneously recording the pressure data from the sensor placed directly into the probe's head the stochastic parts of the signal were eliminated by synchronized sampling of the triggered signal.

2.2.3 Results

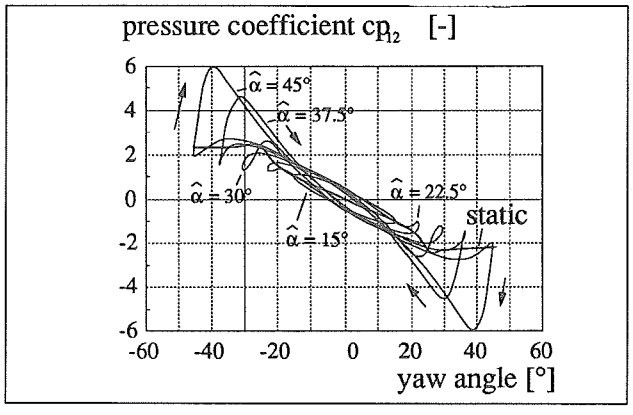

Figure 2-4 *Dynamic calibration of a 60° wedge type probe for a reduced frequency k = 0.10 with different amplitudes of oscillation compared to static calibration data*

An example for dynamic calibration data recorded is given in figure 2-4 showing drastic deviations from the static case. The coefficient cp_{12} for yaw angle measurement is determined by the difference between the opposite sensing holes of the probe:

$$cp_{12} = \frac{p_1 - p_2}{\frac{\rho \cdot u^2}{2}}$$

Note that the dynamic calibration data for higher amplitudes of oscillation exceed the static values. Only for very low amplitudes of fluctuation (well below the static stall angle) do the curves show no hysteresis. For such configurations a linear relation between parameters of fluctuation and experiment can be established (figure 2-5). As the amplitude of the oscillation is increased nonlinear effects dominate the calibration data.

For a comparison of the configurations tested (fig. 2-5) the maximum error-angle $\Delta\alpha_{err}$ (absolute deviation of interpreted flow angle) was determined by:

$$\Delta\alpha_{err} = \left| \frac{cp_{12,\,dynamic} - cp_{12,\,static}}{\left.\frac{dcp_{12,\,static}}{d\alpha}\right|_{\alpha=0}} \right|$$

The equation is valid only for the quasi-linear calibration ranges (where $dcp_{12}/d\alpha$ = const.) but was applied to all ranges leading to an underestimation of the errors in cases where the dynamic values exceed the static calibration range.

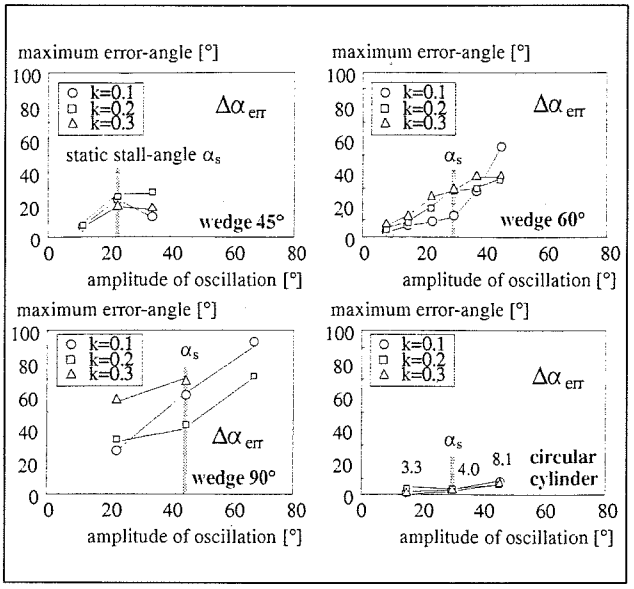

Figure 2-5 *Absolute maximum dynamic error-angles for the configurations tested versus amplitude of oscillation*

To some extent the errors can be seen to be dependent both on amplitude and frequency of oscillation while the geometry drastically affects the dynamic errors. Qualitatively, for the wedge-type configurations (45 & 60°) the errors show an almost linear increase with amplitude of oscillation to approximately half the static stall angle (which is generally of the order of half the apex-angle). From the probe geometries tested the circular cylinder was least affected by dynamic flow phenomena. This is obviously due to the fact that the cylinder itself generates no static lift and is hence less sensitive to added mass effects.

3 SENSOR CHIPS, PACKAGING AND PRESSURE MEASUREMENT ERRORS

3.1 Sensor Chips

The piezoresistive pressure transducers, designed for biomedical applications, are manufactured by silicon micromachining. All its parts (resistors, interconnections and the insulating layers) are fabricated like integrated circuits by a standard planar process. The membrane is formed by anisotropic etching from the rear. The resistors are connected in a conventional Wheatstone-bridge configuration (see figure 3-1).

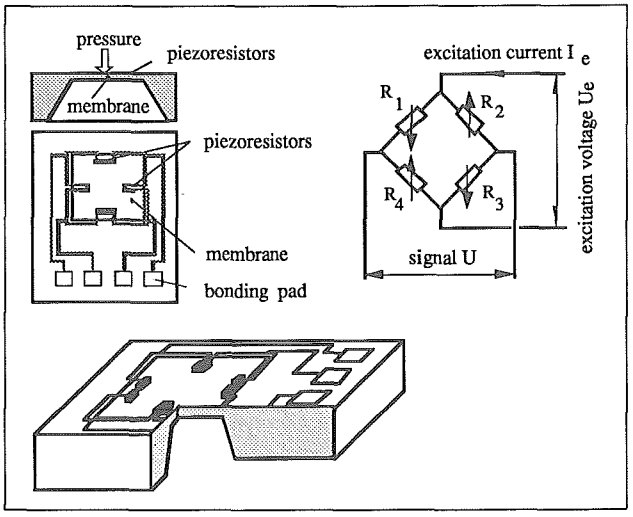

Figure 3-1: *Miniature piezoresistive pressure transducer (the arrows in the circuit diagram indicate the direction of the resistance changes when a pressure p is applied)*

Typical properties of monocrystalline silicon sensor chips are shown in table 3-2. Although the chips are batch-processed they have wide variations in physical properties. For this reason, the purchased sensor chips are individually tested to evaluate their suitability for use in our probes (temperature coefficients of both signal and excitation, stability and thermal hysteresis).

Properties of monocrystalline silicon sensor chips	
Typical dimensions (L / W / H)	1.5 - 2.0 / 0.6 - 1.2 / 0.15 - 0.5 mm
Typical sensitivity	10 - 20 µV/V/mbar
Burst pressure	3 - 20 bar
Max. temp. for measurements	120 °C

Table 3-2: *Typical properties of monocrystalline silicon sensor chips*

3.2 Sensor Packaging

The sensor packaging consists of: mechanical mounting of the chip, electrical connection, electrical insulation and environmental protection of the silicon membrane.

The sensor properties are strongly affected by the packaging technique and the materials used. Most of the undesired effects like creep, thermal hysteresis and thermal transients are caused by improper packaging and can be minimized by:

- selecting the material for the probe body to match the thermal expansion of the sensor chip as close as possible
- "soft bonding" the sensor to the probe using a rubberlike adhesive which reduces strain induced forces
- choosing adhesives with adequate thermal, mechanical and chemical properties.

As a second task, the packaging technique aims to minimize the probe dimensions. Two alternative design types are shown in figure 3-3.

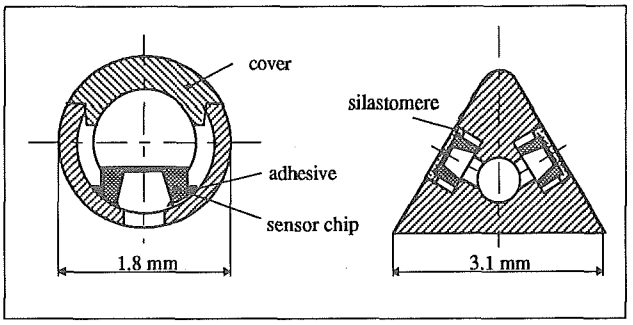

Figure 3-3 *Cylindric and wedge type probe design*

Design 1 with the active side of the diaphragm (with the resistors and electrical connections) turned inside does not require further protection against particle impacts during measurements. However, the pneumatic cavity between the diaphragm and the probe surface reduces the usable frequency range. The manufacturing of probes with design 2 is less complicated than design 1 but requires a more accurate positionning of the sensor chip on the probe surface. A thin layer of silicon rubber protects the active surface of the chip.

3.3. Sensor Properties

A systematic investigation has been performed to minimize the errors of the pressure measurement.

The total error of a measuring system can be divided into *static* and *dynamic* errors; each further subdivided into *systematic* and *random* errors (figure 3-4).

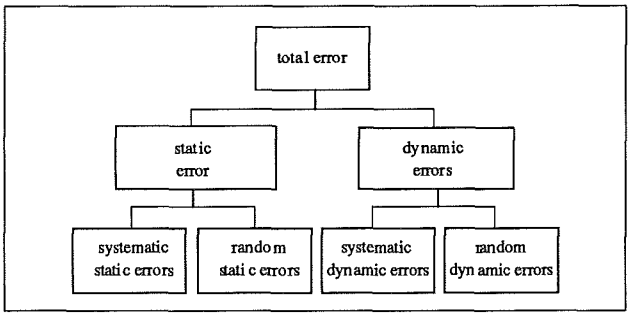

Figure 3-4 *Classification of measurement errors*

To achieve accurate measurements all systematic static errors have to be compensated to a minimum. The remaining systematic errors and also the random errors must be quantified. It is possible to minimize these measurement errors and by adjusting the zero and gain prior to measurement.

3.3.1 Compensation of Systematic Static Errors

The sensor properties can be determined by calibrating the sensors in the desired temperature and pressure range. Conventionally the *thermal* shift of zero and sensitivity are compensated by adding external resistors (NTC and/or PTC) to the Wheatstone bridge of the sensor (EPSTEIN 1985; ICS APPLICATION NOTE 002; MALLON/BERNSTEIN 1983; BOMHOLDT 1983; ENDEVCO TP 268; SCAFER 1989; KOPYSTYNSKI 1989). With the conventional compensation the remaining systematic errors have the following magnitude:

- Deviation from linearity 0.5-1.5% FS (Full Scale)
- Thermal zero shift ± 1-2 % FS / 100 K
- Thermal sensitivity shift ± 1-2 % FS / 100 K

To enhance the accuracy of the pressure measurement a Model Based Reconstruction (MBR) can be used instead of conventional compensation. MBR uses a mathematical model to compensate the errors by computer.

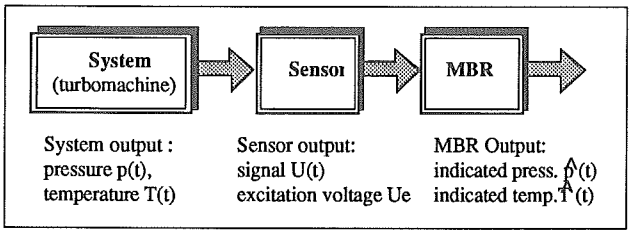

Figure 3-5 *Model based reconstruction*

To perform an MBR the following steps are necessary:

- Calibration of the sensor with constant current excitation. Both the excitation voltage U_e and the signal U are measured as functions of pressure and temperature (figure 3-6).

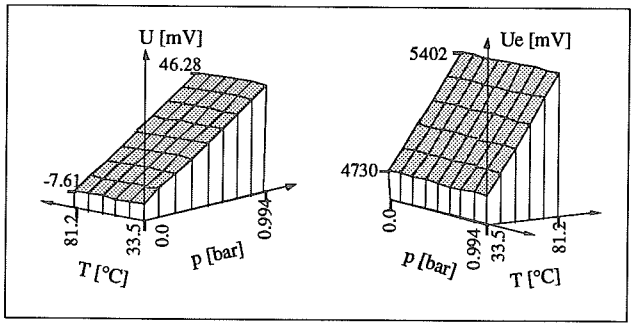

Figure 3-6 *Calibration data of a sensor in the range of $0 \le p \le 1bar; 30°C \le T \le 80°C$*

- With the calibration data an estimate of the parameters c_p and c_T of the model are calculated using least squares approximation. The model describes the relation between the indicated quantities (pressure $\hat{p}$ and temperature $\hat{T}$) the sensor signal U and the excitation voltage U_e:

$$\hat{p} = \sum_{i}^{m} \sum_{j}^{n} c_{pij} U^i U_E^j \qquad \hat{T} = \sum_{i}^{m} \sum_{j}^{n} c_{Tij} U^i U_E^j$$

Normally the number of parameters in the model is less than nine (nine parameters are obtaind by setting m =n =2) (see GOSSWEILER / HUMM / KUPFERSCHMIED 1990).

With this method, both pressure and temperature can be measured with the same sensor. The remaining systematic errors are an order of magnitude smaller compared to conventional compensation. They are typically within ± 0.1 % FS (in the range of $0 \le p \le 1bar$; $30°C \le T \le 80°C$).

3.3.2 Static and Dynamic Random Errors

The most significant errors remaining are random errors due to drift (lacking long term stability), creep, thermal hysteresis and thermal sensor noise.

- The thermal hysteresis is typically less than ± 1 mbar for temperature cycles of 50°C (30-80°C) and is caused by the nonlinear mechanical behaviour of the packaging material used (figure 3-7).

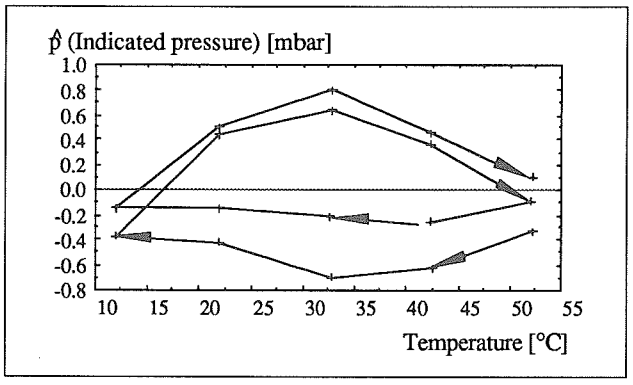

Figure 3-7 *Thermal hysteresis of indicated pressure for two temperature cycles (12 - 52 °C). Additionally a zero drift of 0.4 mbar is also visible.*

- The creep of the signal is less than 0.06 % FS in the range of $0 \le p \le 1bar$ $30°C \le T \le 80°C$ if the sensors are exposed to maximum pressure for 6 minutes. This is much less than the creep measured by COOK 1989 (0.3% FS).

- The long term stability is shown in figure 3-8 where the overall error e_{tot} (sum of all remaining systematic and random errors) in the calibrated range of $0 \le p \le 1bar$ $30°C \le T \le 80°C$ is plotted as a function of time.

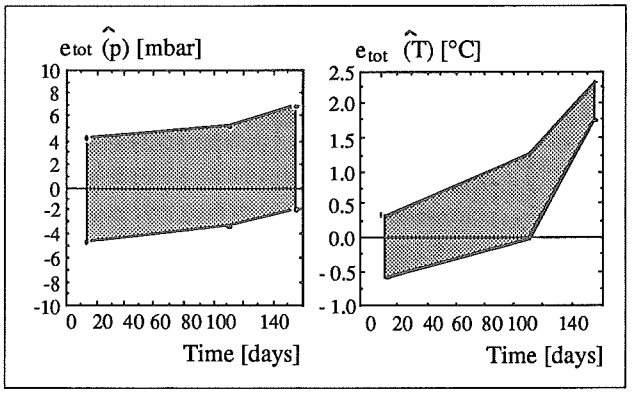

Figur 3-8 *Long term stability of a sensor. The plot shows the total error of the indicated pressure and temperature over a time period of 150 days.*

If the overall error exceeds an acceptable level, the sensors have to be recalibrated. A reduction of stability errors can be obtained by adjusting zero and span shortly before measurements are taken.

• The electrical noise U_n is mainly thermal resistor noise and can be calculated with:

$$U_n^2 = 4\,k\,T\,R\,\Delta f \qquad [V^2]$$

(k = Boltzmann's constant; T = absolute temperature; R = resistance of the Wheatstone bridge; Δf = bandwidth)

At temperatures higher than 120°C semiconductor effects lead to a significant increase of the noise (figure 3-9).

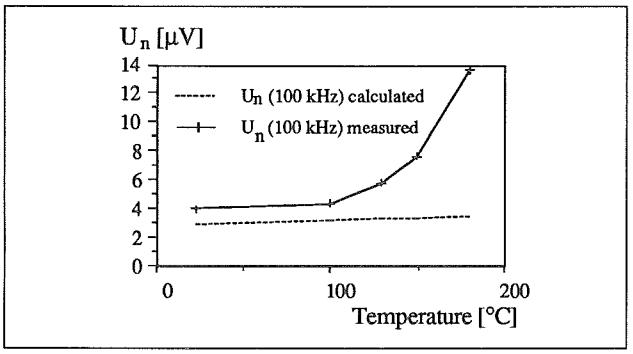

Figure 3-9 *Sensor noise in a bandwidth of 100 kHz*

The sum of sensor and amplifier noise (see sect.5.) limits the resolution of the pressure measurement at low pressure levels.

3.3.3 Systematic Dynamic Errors

The dynamic errors caused by pressure and temperature fluctuations can considerably exceed the static errors.

• Dynamic calibration of pressure transducers

For the dynamic calibration the sensor is exposed to a pressure step generated by means of a shock tube. The frequency response function can be calculated from the sensor signal (figure 3-10).

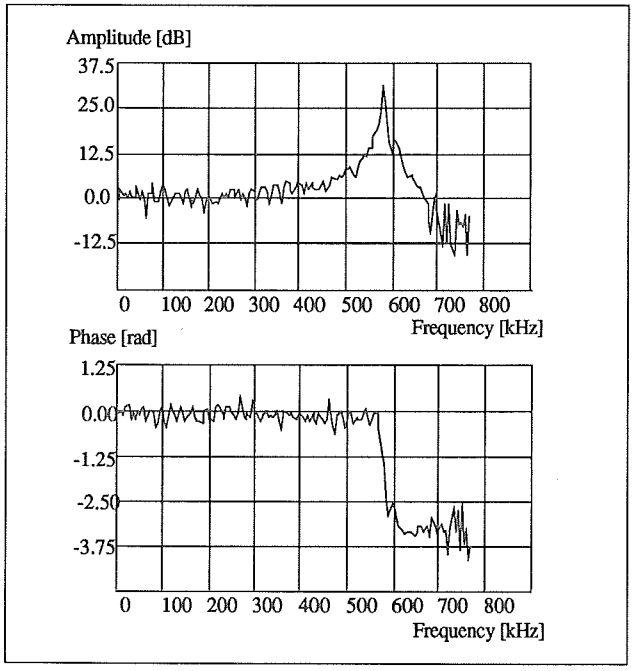

Figure 3-10 *Typical frequency response of a miniature sensor. The natural frequency of the diaphragm is 585 kHz.*

Pneumatic cavities strongly reduce the usable frequency range of the sensor due to resonances of the fluid (GOSSWEILER / HUMM / KUPFERSCHMIED 1990).

• Thermal transient errors

Exposed to thermal transients (e.g.during the start up of a turbomachine) the sensors show large deviations from the static behaviour. The dynamic thermal errors are caused by transient mechanical strains between sensor chip and probe body during the thermal transient. The maximum total error during a temperature step of 50°C is e_{DThmax} = 2 % FS.

4. STATIC AERODYNAMIC PROPERTIES OF MULTIHOLE PROBES

The aerodynamic behaviour of a probe in a flow without time variation of both the direction and the magnitude of the flow vector is denoted in the following as its "static aerodynamic behaviour".

4.1 Probe Geometry

The probe design is strongly dependent on the application. In general, the probe size has to be minimized to increase the spatial definition and the time resolution as well as to reduce the blockage effects, flow perturbations and dynamic aerodynamic errors. The requirements to the probe in the matter of sensitivity and pressure distribution have already been discussed in sect. 2.

For our applications in turbomachines, prismatic probes (i.e. wedge, parabolic or cylindrical type; see figure 4-1) are of special interest, they can be intruded into experimental test rigs through small holes in the casing. Some of these design objectives are incompatible and have to be balanced.

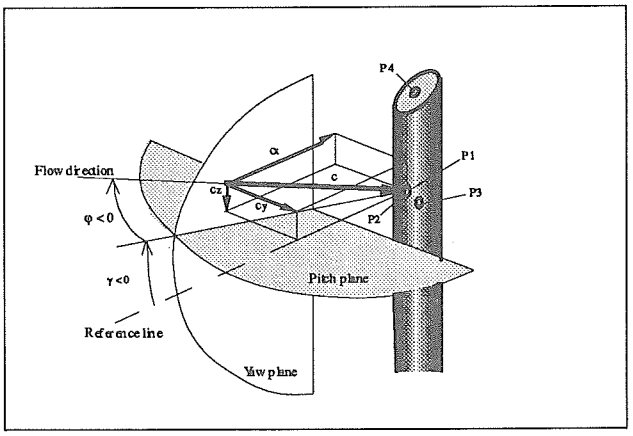

Figure 4-1 *Cylindrical four-hole pressure probe (Ø 2.5 mm) with coordinate system*

4.2 Static Aerodynamic Calibration

The pressure probes were manufactured both in a fast response and in a conventional pneumatic version with the same geometry for aerodynamic tests. Two wind tunnels have been built and are used for general probe investigations and calibrations:

• A free jet test facility, with a jet diameter of 100 mm, is dedicated to probe calibrations under static aerodynamic conditions (as a function of stagnation pressure, pitch and yaw angle, temperature and Mach number)

• A transonic calibration tunnel (nozzle cross section of 200 x 40 mm^2) permits calibrations up to Mach 1.4 as well as investigations on the flow field around probes with holography and other methods.

4.3 Calibration, Models and Aerodynamic Evaluation Procedures

4.3.1. Calibration and Calibration Coefficients

The pressure signals p_i (φ, γ, Ma) obtained for each hole i during calibration under static conditions are transformed into a set of dimensionless calibration coefficients. The choice of these coefficients is mainly dictated by their behaviour in the whole angular range of the flow. An adequate set of coefficients K should be well defined in the interesting angular range, should not contain any mathematical discontinuities and a satisfactory fitting with a model should be possible. Plots of typical dimensionless calibration coefficients K of a cylindrical four hole pressure probe (figure 4-1) are shown in figure 4-2 as a function of pitch and yaw angle (Ma = 0.1).

$$K_1(\gamma, \varphi, Ma) = \frac{p_1 - p_4}{p_1 - \frac{p_2+p_3}{2}} \qquad K_2(\gamma, \varphi, Ma) = \frac{p_{tot} - p_1}{p_1 - \frac{p_2+p_3}{2}}$$

$$K_3(\gamma, \varphi, Ma) = \frac{p_{tot} - p_{stat}}{p_1 - \frac{p_2+p_3}{2}} \qquad K_4(\gamma, \varphi, Ma) = \frac{p_2 - p_3}{p_1 - \frac{p_2+p_3}{2}}$$

The maximum angle without discontinuities of the coefficients K of such a probe ranges between -30° and +30° for both yaw and pitch. Actually, these angle ranges are quite large for applications in turbomachinery and can be tightened to obtain a higher accuracy in the data evaluation.

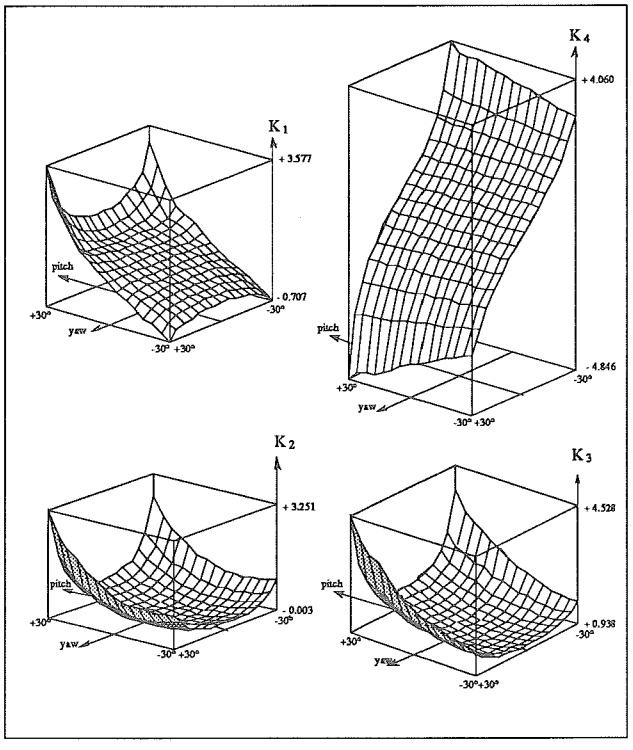

Figure 4-2 *Dimensionless calibration coefficients K_i of a cylindrical four hole pressure probe (Ma = 0.1)*

4.3.2. Modelling of the Calibration Coefficients

For further numerical data processing, a polynomial model $z_M(x, y)$ of a higher degree was found to be a good method to describe such surfaces (RUBNER/BOHN 1972, BOHN/SIMON 1975). In the following discussion and the applications shown in section 6.2, we consider an incompressible flow without Mach number influence:

$$z_M = \sum_{i=0}^{m} \sum_{j=0}^{n} A_{ij}\, x^i\, y^j$$

The degree of the polynomial has to be optimized depending on the geometry of the probe (which influences appreciably the shape of the calibration surfaces) and the angular range of interest.

4.3.3. Data Evaluation

The indicated pressures $\hat{p}_i$ and temperatures $\hat{T}_i$ are used to determine the flow quantities ($\hat{\gamma}$, $\hat{\varphi}$, $\hat{p}_{tot}$, $\hat{p}_{stat}$, $\hat{\rho}$, $\hat{c}$). The indicated flow angles have to be computed first with one of the methods below by solving the model equations:

• *Iterative angle evaluation procedure* ("indirect" method)
The models of the calibration coefficients K_{1M} and K_{4M} are defined as functions of yaw φ and pitch γ:

$$K_{1M} = \sum_{i=0}^{m} \sum_{j=0}^{n} A_{1ij}\, \gamma^i\, \varphi^j$$

$$K_{4M} = \sum_{i=0}^{m} \sum_{j=0}^{n} A_{4ij}\, \gamma^i\, \varphi^j$$

With the pressures $\hat{p}_i$ the coefficients $\hat{K}_1$ and $\hat{K}_4$ are calculated, the unknown angles $\hat{\gamma}$ and $\hat{\varphi}$ are determined iteratively by setting $\hat{K}_1 = K_{1M}$ and $\hat{K}_4 = K_{4M}$.

• *"Direct" angle evaluation procedure*
The aerodynamic behaviour of the described cylindrical four hole probe permits the definition of calibration coefficients by exchanging the dependent and independent variables (figure 4.3) to model the probe properties in a wide spread flow angle range as follow:

$$\gamma_M = \sum_{i=0}^{m} \sum_{j=0}^{n} A_{\gamma ij}\, K_1^{\,i}\, K_4^{\,j}$$

$$\varphi_M = \sum_{i=0}^{m} \sum_{j=0}^{n} A_{\varphi ij}\, K_1^{\,i}\, K_4^{\,j}$$

$\hat{K}_1$ and $\hat{K}_4$ are calculated as described above and the unknown flow angles $\hat{\gamma}$ and $\hat{\varphi}$ can consequently be calculated directly.

The major advantage of the direct method lies in the very short numerical processing time. However, the more ticklish mathematical conditioning of the problem sets limits to certain applications (e.g. special probe geometries, restrictions in flow angle range).

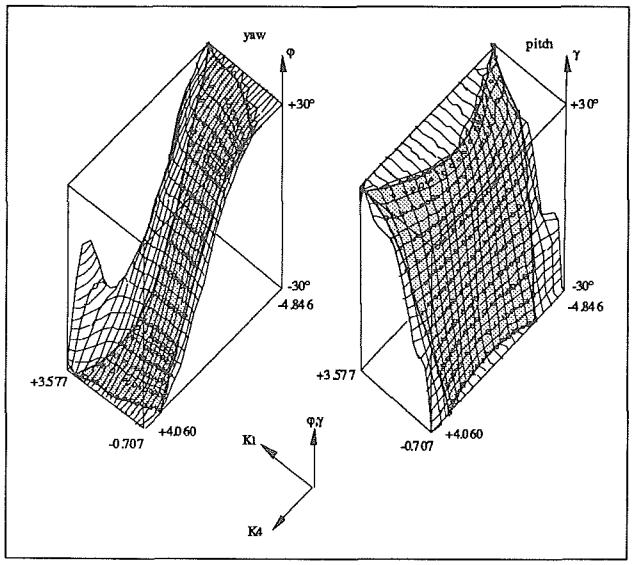

Figure 4-3 *Flow angles γ and φ as functions of dimensionless calibration coefficients K_i (cylindrical four hole pressure probe, Ma = 0.1)*

Afterwards, both total and static pressure are calculated directly from the flow angles (the calibration data $K_2 = F(\gamma,\varphi)$ and $K_3 = F(\gamma,\varphi)$ are also described with the above polynomial model) with:

$$\hat{p}_{tot} = \hat{p}_1 + K_{2M}\left(\hat{p}_1 - \frac{\hat{p}_2+\hat{p}_3}{2}\right)$$

$$\hat{p}_{stat} = \hat{p}_{tot} - K_{3M}\left(\hat{p}_1 - \frac{\hat{p}_2+\hat{p}_3}{2}\right)$$

As shown in section 3.3.1, the pressure as well as the temperature information are obtained from the sensor calibration data. The indicated flow velocity is calculated based on this temperature and both total and static pressure. Finally, an overall iteration loop becomes necessary if the models are Mach number dependent.

5 MEASURING EQUIPMENT AND DATA EVALUATION

5.1 Measuring Equipment

The electric sensor signals of the high frequency response probe are measured, filtered, A/D converted and stored in a specially developed data acquisition system. The system constists essentially of the components shown in figure 5-1 with the technical performances in table 5-2.

5.2 Data Evaluation System

The measured data are evaluated offline in a specially developed software environment running on DEC VAX computers. This software package called "AW-System" has the following most important features:

- VMS-like command-line language with interactive stepwise evaluation of the data. The commands can also be grouped into command procedures to run evaluations as batch jobs
- Efficient memory management and handling of the very large data sets, which are stored in the mainframe virtual memory during the processing in order to minimize I/O-time
- More than 50 commands implemented to carry out data handling, conversion of measured data into physical quantities, statistics, digital signal analysis, digital filtering and graphic output of the results
- Ability to expand the existing system in a simple way by adding new functions or procedures.

Figure 5-3 illustrates the different steps of the interactive evaluation session of four-hole probe measurements in a turbulent pipe flow (see section 6).

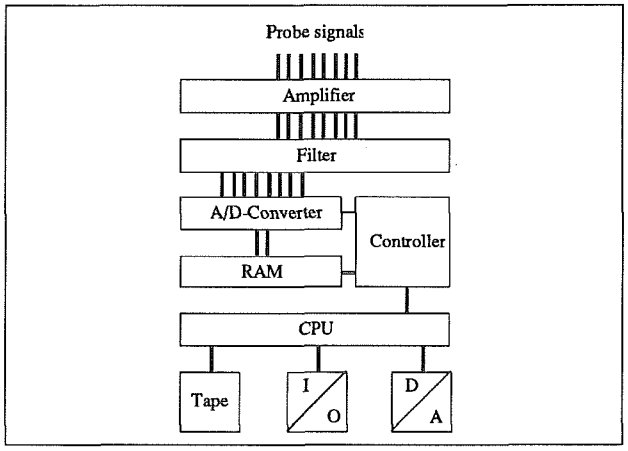

Figure 5-1: *High frequency response measurement and data acquisition system*

High-speed data acquisition system	
Number of channels	8
Sampling rate per channel	max. 200 kHz
Amplifier Type Band-width	differential 470 kHz
A/D converter resolution	12 bit (linearity 11.5 bit)
Initiation reference	provided with 2 extra bits
Low-pass anti-aliasing filter	eight-pole Butterworth (48dB/octave) and allpass filter for phase correction. Gain accuracy ≈ 1% up to 40 kHz
CPU	DEC MicroVAX
Dynamic memory system	on-line storage into RAM, capacity 2 MWord/channel
Data storage	hard-disk or tape

Figure 5-2: *Performances of the data acquisition system*

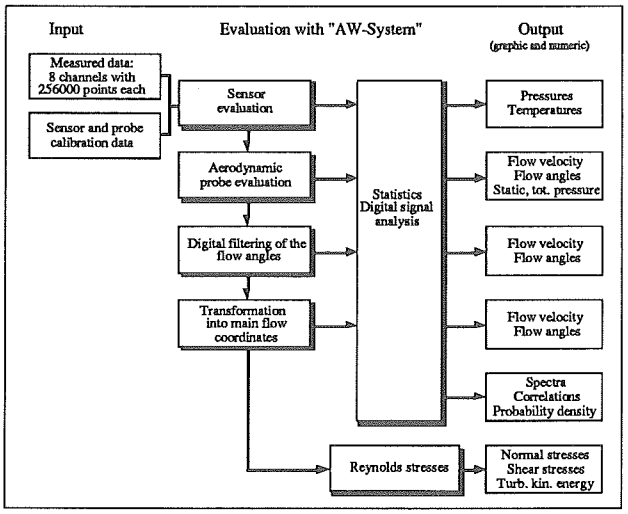

Figure 5-3: *Evaluation steps of measurements in a turbulent pipe flow*

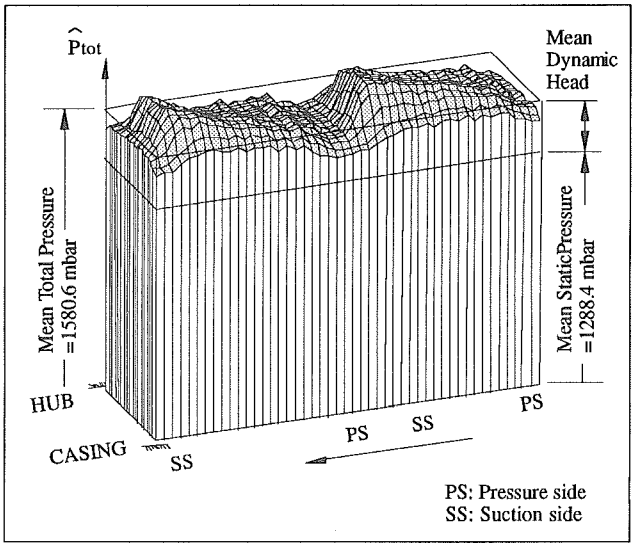

Figure 6-2: *Time dependent total pressure distribution*

A rough determination of the yaw angle fluctuation $\widehat{\varphi}'(t)$ (figure 6-3) was made possible by yawing the probe alternately in each direction by 45° and then applying the static calibration data .

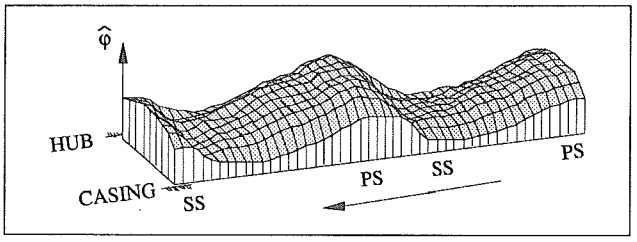

Figure 6-3: *Time dependent flow angle distribution. The yaw angle φ fluctuates between 16 and 33°.*

Both tangential and radial velocity components are determined from this data. Figure 6-4 shows the radial velocity C_r at two different radial positions r/r_{wheel} = 1.05 and 1.16 in the diffuser. It can be seen clearly that the systematic fluctuations caused by the impeller decay very rapidly downstream.

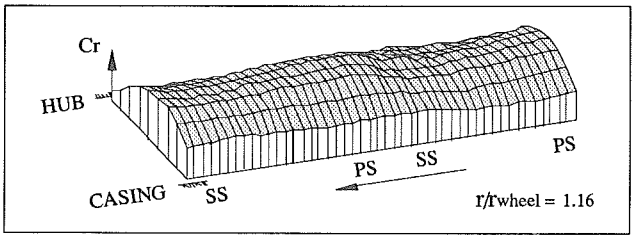

Figure 6-4 *Decay of systematic fluctuations of the radial velocity in the diffuser.*

The measurements in the radial compresser revealed a high probe reliability. Although no protective layer was applied to the diaphragm of the sensor more than 100 operating hours have been carried out in a highly turbulent flow at Mach numbers up to 0.75 and temperatures up to 80°C without damage or changes of sensitivity.

6 APPLICATIONS

Two different applications are discussed to give a practical illustration of the techniques described in the sections above:
i) Investigations on the systematic fluctuations of the flow vector at the exit of a radial compressor impeller
ii) Measurement of the time dependent flow vector in a fully developed pipe flow.

6.1 Measurements in the Diffuser of a Radial Compressor

The flow at the exit of the impeller was measured at several radial positions in the diffuser to quantify the systematic fluctuations (HUNZIKER/RIBI/SPIRIG/GYARMATHY 1990). Technical data of the radial compressor are listed in table 6-1.

Diameter of impeller:	280 mm	Max. tip Mach number:	M_u = 0.75
Diffuser width :	17 mm	Typical pressure ratio:	1.5
Number of blades:	18	Typ. blade passing freq.:	6.5 kHz

Table 6-1: *Technical data of the radial compressor*

The time averaged flow velocity and direction have been measured first with a conventional cylindrical two hole pressure probe (Ø 1.8 mm). Measurements of the systematic fluctuations caused by blade passing have been taken with a fast response probe (Ø 1.8 mm, equipped with a single pressure sensor) and with a flush mounted pressure transducer. Phase locked sampling and ensemble averaging was used for the data reduction (HUNZIKER et al. 1990). The total pressure fluctuations $\widehat{p}'_{tot}(t)$ have been determined by yawing the probe towards the time averaged main flow direction. The total pressure signal $\widehat{p}_{tot}(t)$ was calculated by superposing the time averaged total pressure and the fluctuation $\widehat{p}'_{tot}(t)$ (figure 6-2). The static wall pressure $\widehat{p}_{stat}(t)$ measured at the same radial position was used to determine the dynamic head $\widehat{q}(t)$.

6.2 Measurements in a Turbulent Pipe Flow

The flow vector (C(t), φ(t), γ(t)) of a fully turbulent pipe air flow was measured using the four sensor fast response probe (figure 4-1). Statistical quantities such as probability distributions, spectra and autocorrelations as well as turbulence level, turbulent kinetic energy and Reynolds stresses have been calculated from this data and some typical results are presented below.

6.2.1 Experimental set up

The measurements were taken in a 10 m long pipe (diameter D = 0.2 m). The time averaged velocity profiles at the exit of the pipe were measured with a conventional pitot tube (Ø 1 mm). The friction velocity was determined by the static pressure drop along the pipe axis .

For our tests the average speed U_{max} at the center was approximately 70 m/s (Ma ≈ 0.2, $Re_D \approx 800{,}000$). The fast response probe was intruded 0.2 m upstream the exit in radial direction. The data acquisition and reduction was made using the equipment and software described in section 5.

6.2.2 Results of the fast response measurements

a) Measurement of time averaged velocity

After rough corrections for the blockage, wall proximity effects and shaft influence, the error of the indicated time averaged velocity of the four sensor probe measurement data was less than ±2 m/s (±2.5 % of U_{max}). Better aerodynamic corrections could reduce these errors because the accuracy of the pressure measurement was typically ±0.75 % of the dynamic head.

b) Measurement of turbulence quantities

The relative turbulence intensities $\sqrt{\overline{u'^2}} / \overline{U}_{max}$ are shown in figure 6-5. Compared to the data of LAUFER 1954 the intensities measured with the four sensor probe are systematically higher with a maximum of 15%.

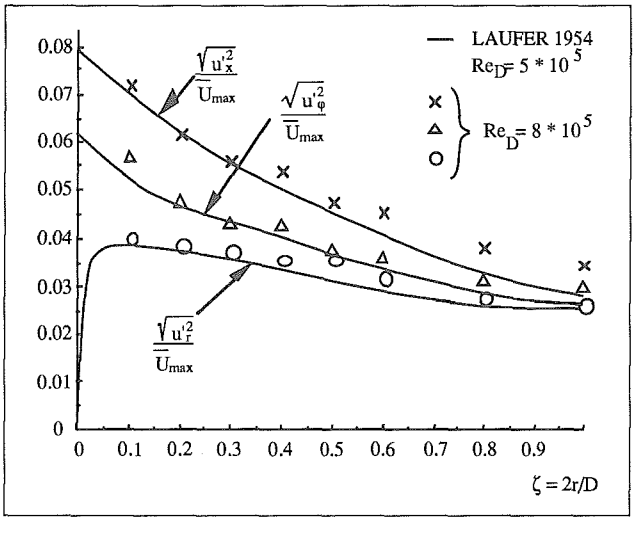

Figure 6-5 *Relative turbulent intensities (see HINZE 1975, p. 725)*

Thus the normal Reynolds stresses and the turbulent kinetic energy could be measured to an acceptable accuracy. But so far it was not possible for us to measure the shear stresses correctly.

Figure 6-6 compares the probability density distribution p^d of u'_x at different relative radii ζ = 2r/D = 1.0, 0.5, 0.1; all of them show a slight negative skewness. The normalized wave number spectrum of u'_x is plotted in figure 6-8. The probability density distribution p^d of total and static pressure fluctuations are shown in figure 6-7.

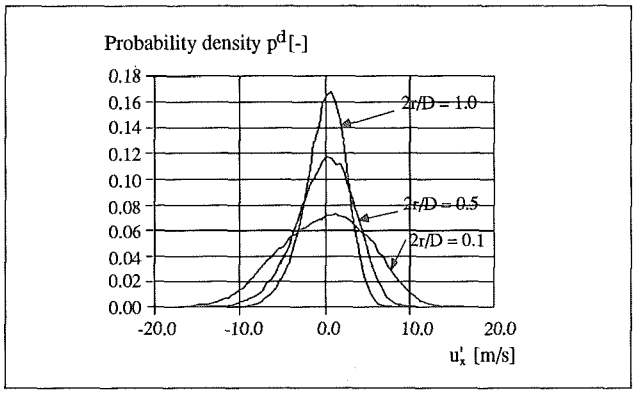

Figure 6-6 *Probability density distribution of u'_x*

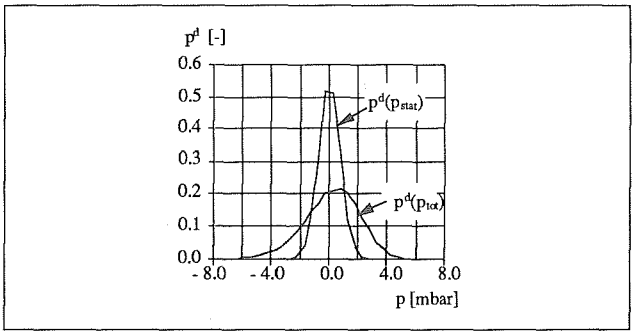

Figure 6-7 *Probability density distribution of total and static pressure fluctuations*

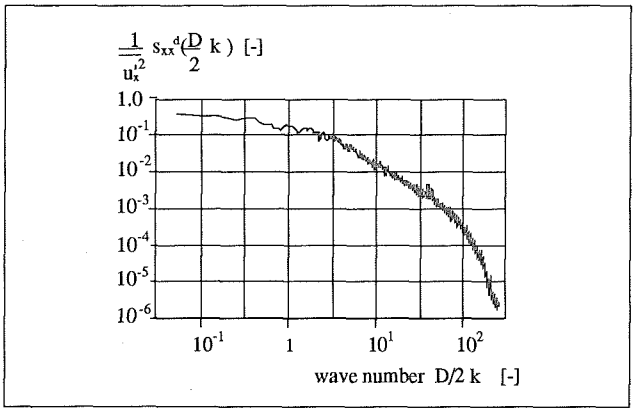

Figure 6-8 *Spectral density $s_{xx}{}^d$ of u'_x. (Directly comparable to HINZE 1975 p.738).*

By integrating the autocorrelation of u'(t) and scaling with the average flow speed $\overline{U}$ the integral length scale can be calculated

L_I = 72 mm. This value lies close to those given by HINZE 1975 ($L_I \approx 0.8 \cdot D/2 = 80$ mm).

Although the air flow passes through a microscopic filter at the pipe inlet, the sensitivity of hot wires used previously to measure the turbulence level decreased about 10 % per operating hour due to dust particle deposition on the wire surface. The fast response probe measurements were not affected by dust or particles and they are much more robust in action.

Acknowledgements

This work is supported by the Swiss National Science Fund SNF (Schweizerischer Nationalfonds zur Förderung der wissenschaftlichen Forschung).

The authors would like to express their sincere appreciation to Prof. G. Gyarmathy, Mr. R. Hunziker, B. Ribi, M. Spirig for making available the presented results from the radial compressor test rig, Dr. D. Herter and Mr. N. O. Chrisander for the development of the software of the data evaluation system and to Mr. C. Reshef for the development of the electronic equipment.

Symbols and Abbreviations

A		polynomial matrix
D	[m]	diameter
c, u	[m/s]	velocity
cp	[-]	nondimensional pressure coefficient
d	[m]	diameter of probe
f	[Hz]	frequency of oscillation
k	[-]	reduced frequency
K	[-]	calibration coefficients
l/L	[-]	rel. pos. of sensing hole to probe length
L_I	[m]	Integral lenght scale
Ma	[-]	Mach number
p	[pa]	pressure
p^d	$[x^{-1}]$	estimate of probability density distribution
PS		pressure side
r	[m]	radius of probe
R	[Ω]	resistance
SS		suction side
$s_{xx}{}^d$	$[x^2/Hz]$	estimate of autospectral density of x'
T	[°C]	temperature
U	[mV]	sensor signal
U_e	[V]	excitation voltage
U,V,W	[m/s]	velocity components (main stream coord.)
$\overline{x'^2}$	[x2]	estimate of the variance of x'
z	[-]	relative radius z = r/rwheel
γ	[°]	pitch angle
$\Delta\alpha_{err}$	[°]	error-angle
φ, α	[°]	yaw angle
ρ	$[kg/m^3]$	density

Indices / Superscripts

err	error
dynamic	dynamic motions
M	model
max	maximum
tot	total
s, stat	static
wheel	radial compressor wheel
0	total
$\hat{x}$	indicated, amplitude of oscillation
x'	fluctuating part
$\bar{x}$	time average

References

BEDDOES T.S.
A Qualitative Discussion of Dynamic Stall;
AGARD-R-679, Special Course on Unsteady Aerodynamics 1980

BOHN, D.; SIMON H.
Mehrparametrige Approximation der Eichräume und Eichflächen von Unterschall- bzw. Ueberschall-5-Lochsonden
ATM Messtechnische Praxis 3. 1975

CARR L.W., MCALLISTER W.J., MCCROSKEY W.J.
Analysis of the Development of Dynamic Stall based on Oscillating Airfoil Experiments
NASA TN D-8382; 1977

EPSTEIN A.L.
High Frequency Response Measurements in Turbomachinery
VKI Lecture Series Brussels 1985-03

GOSSWEILER C., HUMM H.J., KUPFERSCHMIED P.
The Use of Piezoresistive Semiconductor Pressure Transducers for Fast Response Probe Measurements in Turbomachines
Measuring Techniques for Transonic and Supersonic Flows in Cascades and Turbomachines, Proc. 10th Symp. VKI Sept. 1990

GOSSWEILER C., HUMM H.J., KUPFERSCHMIED P.
Dynamic Calibration of Piezoresistive Pressure Transducers in the Frequency Range of over 500 kHz
Proc. Micromechanics Europe 1990, Berlin

HENEKA A.
Entwicklung und Erprobung einer Keilsonde für instationäre dreidimensionale Strömungsmessung in Turbomaschinen
Mitteilung des Inst. für Thermische Strömungsmaschinen der Universität Stuttgart Nr. 14, 1983

HINZE, J. O.
Turbulence
McGraw-Hill New-York 1975

HUNZIKER R., RIBI B., SPIRIG M., GYARMATHY G.
On the Influence of Different Impellers on a Radial Compressor Stage with vaneless Diffuser
Interfluid Essen FRG 1990

GYARMATHY G., HUNZIKER R., RIBI B., SPIRIG M.
On the Change of Impeller Flow Non-Uniformities with Flow Rate in a Centrifugal Compressor
IMechE 1991

KERREBROCK J.L., EPSTEIN. A.H., THOMPKINS W.T.
A Miniature High Frequency Sphere Probe
Proceedings of ASME Symposium on Measurement Methods in Rotating Components of Turbomachinery; 1980,

KOVASZNAY L.S.G., TANI I., KAWAMURA M., FUJITA H.
Instantaneous Pressure Distribution Around a Sphere in Unsteady Flow;
Journal of Fluids Engineering Vol. 103;1981

MATSUNAGA S., ISHIBASHI H., NISHI M.
Accurate Measurement of Non-Steady Three-Dimensional Incompressible Flow by Means of a COmbined Five-Hole Probe
Non-Steady Fluid Dynamics, Winter ASME Meeting 1978

MCCROSKEY W.J.
Some Current Research in Unsteady Fluid Dynamics
THE 1976 FREEMAN SCHOLAR LECTURE;
Journal of Fluids Engineering 99; 1977

NASH J.F., SCRUGGS R.M.
Unsteady Boundary Layers with Reversal and Separation
AGARD CP 227; 1978

RUBNER K.; BOHN D.
Verfahren für die Auswertung der Messergebnisse von Strömungssonden durch mehrparametrige Approximation der Eichkurven und Eichflächen
Z. Flugwiss. 20 1972 Heft 1/2

SARPKAYA T.
Oscillating Flow About Cylinders: Experiments and Analysis
Forum on Unsteady Flow Separation ASME VI/1987

SEARS W.R., TELIONIS D.P.
Boundary-Layer Separation in Unsteady Flows
SIAM Journal on Applied Mathematics, Vol. 28, No. 1, 1975

SHREEVE R.P., NEUHOFF F.
Measurements of the Flow From a High-Speed Compressor Rotor Using a Dual Probe Digital Sampling (DPDS) Technique
Journal of Engineering for Gas Turbines and Power Vol. 106, 1984,

TELIONIS D.P.
Unsteady Viscous Flow;
SPRINGER New York; 1981